PLOS ONE

RESEARCH ARTICLE

The PrpF protein of *Shewanella oneidensis* MR-1 catalyzes the isomerization of 2-methyl-*cis*-aconitate during the catabolism of propionate via the AcnD-dependent 2-methylcitric acid cycle

Christopher J. Rocco[1¤a], Karl M. Wetterhorn[2], Graeme S. Garvey[2¤b], Ivan Rayment[2], Jorge C. Escalante-Semerena[3]*

1 Department of Bacteriology, University of Wisconsin–Madison, Madison, WI, United States of America,
2 Department of Biochemistry, University of Wisconsin–Madison, Madison, WI, United States of America,
3 Department of Microbiology, University of Georgia, Athens, GA, United States of America

¤a Current address: Center for Microbial Pathogenesis, The Research Institute at Nationwide Children's Hospital, Columbus, OH, United States of America
¤b Current address: Monsanto Vegetable Seeds, Woodland, CA, United States of America
* jcescala@uga.edu

OPEN ACCESS

Citation: Rocco CJ, Wetterhorn KM, Garvey GS, Rayment I, Escalante-Semerena JC (2017) The PrpF protein of *Shewanella oneidensis* MR-1 catalyzes the isomerization of 2-methyl-*cis*-aconitate during the catabolism of propionate via the AcnD-dependent 2-methylcitric acid cycle. PLoS ONE 12(11): e0188130. https://doi.org/10.1371/journal.pone.0188130

Editor: Claudio M. Soares, Universidade Nova de Lisboa Instituto de Tecnologia Quimica e Biologica, PORTUGAL

Received: July 20, 2017

Accepted: November 1, 2017

Published: November 16, 2017

Data Availability Statement: All relevant data are within the paper and its Supporting Information file.

Funding: This work was supported by National Institute of General Medical Sciences (https://www.nigms.nih.gov/Pages/default.aspx), grant R01 GM062203 to JCES; National Institute of Allergy and Infectious Diseases (https://www.niaid.nih.

Abstract

The 2-methylcitric acid cycle (2-MCC) is a common route of propionate catabolism in microorganisms. In *Salmonella enterica*, the *prpBCDE* operon encodes most of the 2-MCC enzymes. In other organisms, *e.g.*, *Shewanella oneidensis* MR-1, two genes, *acnD* and *prpF* replace *prpD*, which encodes 2-methylcitrate dehydratase. We showed that together, *S. oneidensis* AcnD and PrpF (*So*AcnD, *So*PrpF) compensated for the absence of PrpD in a *S. enterica prpD* strain. We also showed that *So*AcnD had 2-methylcitrate dehydratase activity and that PrpF has aconitate isomerase activity. Here we report *in vitro* evidence that the product of the *So*AcnD reaction is an isomer of 2-methyl-*cis*-aconitate (2-MCA], the product of the *Se*PrpD reaction. We show that the *So*PrpF protein isomerizes the product of the AcnD reaction into the PrpD product (2-MCA], a known substrate of the housekeeping aconitase (AcnB]. Given that *So*PrpF is an isomerase, that *So*AcnD is a dehydratase, and the results from *in vivo* and *in vitro* experiments reported here, it is likely that 4-methylaconitate is the product of the AcnD enzyme. Results from *in vivo* studies using a *S. enterica prpD* strain show that *So*PrpF variants with substitutions of residues K73 or C107 failed to support growth with propionate as the sole source of carbon and energy. High-resolution (1.22 Å) three-dimensional crystal structures of $PrpF^{K73E}$ in complex with *trans*-aconitate or malonate provide insights into the mechanism of catalysis of the wild-type protein.

gov), grant R21 AI082916 to JCES; National Institute of General Medical Sciences (https://www.nigms.nih.gov/Pages/default.aspx), grant R01 GM086351 to IR.

Competing interests: The authors have declared that no competing interests exist.

Introduction

The 2-methylcitric acid cycle (2-MCC) (Fig 1) is widely distributed route of propionate catabolism in microorganisms. Originally identified in the fungus *Candida lipolytica* (*Yarrowia lipolytica*) [1], the 2-MCC has been characterized in Gamma-proteobacteria (*e.g.*, *Salmonella enterica*, *Escherichia coli*) [2–4], actinobacteria (*e.g. Mycobacterium tuberculosis*, *Mycobacterium smegmatis*, *Corynebacterium glutamicum*) [5–9], and Beta-proteobacteria (*e.g. Ralstonia eutropha*, *Burkholderia sacchari*) [10, 11]. Most of the enzymes that comprise the 2-MCC are encoded as an operon [12]. In *S. enterica* (and many other bacteria), the operon consists of four genes, in the order *prpBCDE*. *prpB* encodes 2-methylisocitrate lyase (EC 4.2.1.99) [2, 13, 14]; *prpC* encodes the 2-methylcitrate synthase (EC 2.3.3.5) (2); *prpD*, encodes the 2-methylcitrate dehydratase (EC 4.2.1.79) [15]; and *prpE* encodes the propionyl-CoA synthetase (EC 6.2.1.17) [16, 17].

There is one notable variation in bacterial *prp* operons. That is, some *prp* operons lack the 2-methylcitrate dehydratase *prpD*, but rather contain two other genes, *acnD* and *prpF* [15]. AcnD has aconitase-like activity [18], whilst PrpF has aconitate isomerase activity [19] (Fig 1). In *S. oneidensis* the sequence of *prp* genes is *prpR prpB prpC acnD prpF* compared to the *S. enterica* sequence *prpR prpB prpC prpD prpE*. In *S. oneidensis*, the *prpE* gene encoding propionyl-CoA synthetase is >1.5 Mbp away from the *prp* operon. AcnD and PrpF activities are necessary and sufficient to compensate for the lack of PrpD during growth with propionate of a *prpD* strain of *S. enterica* [18].

Structural and biochemical analyses of *Shewanella oneidensis* PrpF (hereafter *So*PrpF), revealed a role of *So*PrpF in the isomerization of *trans*-aconitate to *cis*-aconitate [19], leading us to propose that the role of *So*PrpF in the 2-MCC was to change the stereochemistry of the *S. oneidensis* AcnD (hereafter *So*AcnD) reaction product. That is, *So*PrpF was proposed to have 2-methylaconitate isomerase activity [19].

Herein we specifically address the hypothesis that the *S. oneidensis* PrpF (*So*PrpF) protein isomerizes the product of the *So*AcnD dehydratase (putatively 4-methyl-*cis*-aconitate (4-MCA) to 2-methyl-*cis*-aconitate (2-MCA), the substrate of aconitase A, B. To facilitate this work, we used a *S. enterica* Δ*prpD* carrying the wild-type allele of the *S. oneidensis acnD* gene. Into the *S. enterica* Δ*prpD* / p*acnD*$^+$ (*S. oneidensis*) strain we introduced a second plasmid encoding wild-type or variants of *S. oneidensis* PrpF (*So*PrpF). In this heterologous system, PrpF functionality was assessed *in vivo* under conditions that demanded propionate utilization as the sole source of carbon and energy, or a combination of propionate and succinate, which would allow us to assess the effect of the accumulation of 4-MCA on growth in the presence of functional or dysfunctional PrpF proteins.

Materials and methods

Chemicals and bacteria culture media

All chemicals were purchased from Sigma Chemical Co. unless otherwise stated. 2-Methylcitrate was purchased from CDN Isotopes (Pointe-Claire, Canada). Authentic 2-methyl-*cis*-aconitate was custom synthesized by AsisChem (Cambridge, MA). The experiments reported here were performed in well-characterized *S. enterica prp* mutant strains. A previous report from our laboratory showed that this approach allowed us to assess *S. oneidensis* AcnD and PrpF functions *in vivo* [18]. *E. coli* strains used to overproduce recombinant proteins were grown in lysogeny broth (LB) [20, 21]. No-carbon essential (NCE) medium [22, 23] was used as minimal medium, and was supplemented with $MgSO_4$ (1 mM) and methionine (0.5 mM). When added to rich medium, antibiotic concentrations were: ampicillin (100 μg/ml),

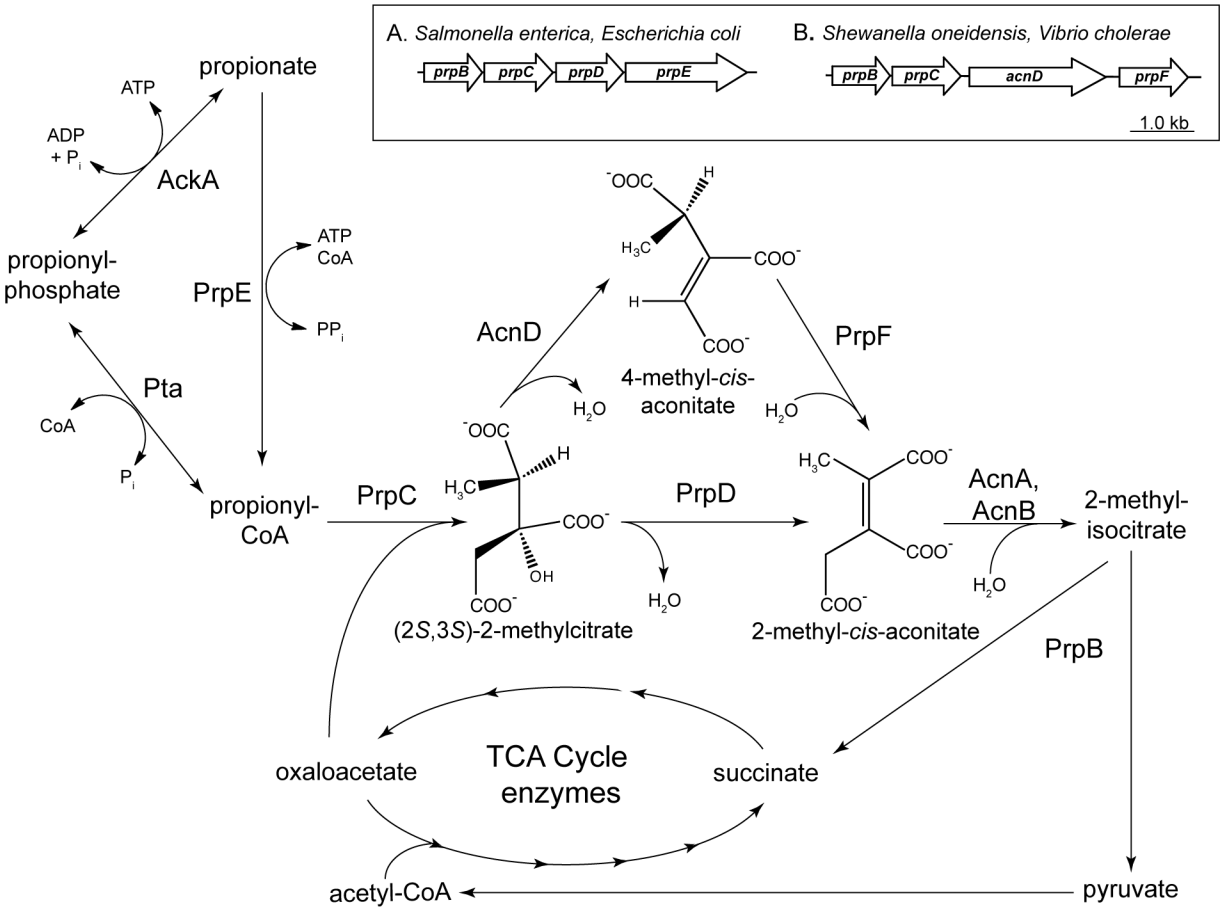

Fig 1. The 2-methylcitric acid cycle. In this metabolic pathway propionate is oxidized to pyruvate with succinate as byproduct. Inset box–difference in operon structure of *Salmonella enterica* and *Escherichia coli* (Inset box A) compared to *Shewanella oneidensis* and *Vibrio cholera* (Inset box B). AckA–acetate kinase; Pta–phosphotransacetylase; AcnA/B–aconitase A, aconitase B.

https://doi.org/10.1371/journal.pone.0188130.g001

kanamycin (50 μg/ml), and chloramphenicol (25 μg/ml). Bacto™ Agar (Difco, 1.5% w/v) was used as medium solidifying agent.

For cloning purposes, restriction endonuclease NdeI was purchased from Fermentas (Glen Burnie, MD), and BamHI was purchased from Promega (Madison, WI). Cloning was performed in *E. coli* strain DH5α/F' (New England Biolabs). Plasmids were introduced into *S. enterica* strains by electroporation. Cultures were grown in LB medium to an optical density (650 nm) ~0.6–0.8, 1.0 ml of culture was centrifuged at 18,000 x *g* using a Microfuge 18 Centrifuge (Beckman Coulter), cells were washed three times with 1.0 ml of ice-cold sterile water, and re-suspended in 100 μl of water. Plasmids were electroporated into cells using a Bio-Rad Gene Pulser (Hercules, CA) according to the manufacturer's recommendations. Strains and plasmids used in this study are listed in Table 1.

Site-directed mutagenesis

All site-directed mutations were introduced into targeted genes using the QuikChange® II XL Site-Directed Mutagenesis Kit (Stratagene); all manipulations of plasmids carrying wild-type or mutant alleles of genes of interest were performed in XL10 Gold® Ultracompetent *E. coli* cells (Stratagene).

Table 1. Strains and plasmids used in this study.

Strain	Relevant genotype	Source
***E. coli* strains**		
BL21(λDE3)	F$^-$ *ompT hsdS$_B$* (r_b^- m_b^+) *dcm gal* I(DE3)	New England Biolabs
DH5α/F'	F'/*endA1 hsdR17* (r_k^- m_k^+) *supE44 thi-1 recA1 gyrA* (Nal^r) *relA1* Δ(*lacZYA-argF*)*U169 deoR* [f80d*lac*D (*lacZ*)*M15*]	New England Biolabs
XL10-Gold® Ultracompetent cells	TetR Δ(*mcrA*)183Δ(*mcrCB-hsdSMR-mrr*)173 *endA1 supE44 thi-1 recA1 gyrA96 relA1 lac* Hte [F' *proAB lacIqZΔM15* Tn*10* (TetR) Amy CamR]a	Stratagene
***S. enterica* strains**		
TR6583	*metE205 ara-9*	K. Sanderson via J. Roth
Derivatives of TR6583		
JE8250	*prpD126*::*cat*$^+$	This work
JE8256	JE8250 / pPRP138	This work
JE8429	JE8256 / pPRP153	This work
JE9373	JE8256 / pPRP215 *prpF255*	This work
JE9374	JE8256 / pPRP216 *prpF256*	This work
JE9592	JE8256 / pPRP218 *prpF257*	This work
JE9593	JE8256 / pPRP219 *prpF258*	This work
JE11597	JE8256 / pPRP223 *prpF259*	This work
Plasmids		
pPRP138	*S. oneidensis acnD*$^+$ in pBAD30 *bla*$^+$	[18]
pPRP153	*S. oneidensis prpF*$^+$ in pBAD18Kan *kan*$^+$	[18]
pPRP195	*S. oneidensis acnD*$^+$ cloned into pET-15b *bla*$^+$	This work
pPRP196	*S. oneidensis prpF*$^+$ cloned into pTEV4 *bla*$^+$	[19]
pPRP205	*S. oneidensis acnD*$^+$ cloned into pTEV5	This work
pPRP215	*S. oneidensis prpF*$^+$(*prpF255* C107A) in pBAD18Kan *kan*$^+$	This work
pPRP216	*S. oneidensis prpF*$^+$(*prpF256*; encodes PrpF^{C107S}) cloned into pBAD18-Kan *kan*$^+$	This work
pPRP217	*S. oneidensis prpF*$^+$(*prpF255*; encodes PrpF^{C107A}) cloned into pTEV4 *bla*$^+$	This work
pPRP218	*S. oneidensis prpF*$^+$(*prpF257*; encodes PrpF^{K73A}) cloned into pBAD18-Kan *kan*$^+$	This work
pPRP219	*S. oneidensis prpF*$^+$(*prpF258*; encodes PrpF^{K73E}) cloned into pBAD18-Kan *kan*$^+$	This work
pPRP220	*S. oneidensis prpF*$^+$(*prpF257*; encodes PrpF^{K73A}) cloned into pTEV4 *bla*$^+$	This work
pPRP221	*S. oneidensis prpF*$^+$(*prpF258*; encodes PrpF^{K73E}) cloned into pTEV4 *bla*$^+$	This work
pPRP223	*S. oneidensis prpF*$^+$(*prpF259*; encodes PrpF^{K73M}) cloned into pBAD18-Kan *kan*$^+$	This work
pET-15b	Cloning vector pBR origin of replication *bla*$^+$; fuses a thrombin-cleavable H_6 tag to the N-terminus of the protein of interest	Novagen
pTEV4	Cloning vector; F1 origin of replication *bla*$^+$; fuses a TEV-cleavable H_6 tag to the N-terminus of the protein of interest	[24]
pTEV5	Cloning vector; F1 origin of replication *bla*$^+$; fuses a TEV-cleavable H_6 tag to the N-terminus of the protein of interest	[24]
pBAD30	Cloning vector; pACYC184 origin of replication, *bla*$^+$; expression of the gene of interest under the control of the arabinose-inducible P_{araBAD} promoter	[46]
pBAD18-Kan	Cloning vector; pBR origin of replication, *kan*$^+$; expression of the gene of interest under the control of the arabinose-inducible P_{araBAD} promoter	[46]

https://doi.org/10.1371/journal.pone.0188130.t001

Polymerase chain reaction (PCR)

Amplification conditions for site-directed mutagenesis were as follows: 95˚C for 1 min, followed by 19 cycles of 95˚C for 50 s, 60˚C for 50 s, 68˚C for 6 min 15 s, ending with 68˚C for 7 min. All plasmids carrying mutant *S. oneidensis prpF* alleles were sequenced using two described primers [19]. DNA sequencing reactions were performed using BigDye® (Applied Biosystems), were purified using CleanSEQ protocols (Agentcourt Biotechnology), and were resolved at the University of Wisconsin-Madison Biotechnology Center.

Plasmid pPRP195

The *S. oneidensis acnD*$^{+}$ gene was amplified from plasmid pPRP141 (18) using primers `5′–GTT ATG AGC ACA CAT ATG AAC ACC CAA TAT C– 3′ and 5′ –GAT ATA GGC GGG ATC CAT GTC GGC ATT GC–3′.` The resulting DNA fragment (~2.5 kb) was extracted from the gel using the QIAQuick Gel Extraction kit (Qiagen), the fragment was digested with NdeI and BamHI, and ligated into plasmid pET-15b (*bla*$^{+}$) digested with the same enzymes; the resulting plasmid (pPRP195) was electroporated into *E. coli* DH5α/F', and cells were plated onto LB + ampicillin medium.

Plasmid pPRP205

Plasmid pPRP195 was digested with NdeI and BamHI; the fragment containing the *S. oneidensis acnD*$^{+}$ allele was extracted from the gel as described above. The fragment was ligated into plasmid pTEV5 [24] digested with the same enzymes. The resulting plasmid (pPRP205) was electroporated into *E. coli* DH5α/F', and cells were plated onto LB + ampicillin medium.

Plasmids pPRP215-226

Plasmids pPRP153 [18] and pPRP196 [19] were used as templates to generate single-amino acid variants of the *So*PrpF protein with the QuikChange® II XL Site-Directed Mutagenesis kit (Stratagene). Other information pertinent to the construction of these plasmids is summarized in Table 2.

Isolation of proteins

*So*PrpF protein was purified as described [19]. Variant *So*PrpF proteins were purified using the Maxwell™ 16 system (Promega). Cultures were grown in LB + ampicillin at 37˚C, and induced

Table 2. List of plasmids encoding PrpF variants used in this study.

Plasmid	Allele #	Primers 5'– 3'	Template	Protein Encoded
pPRP215	*prpF255*	GTGGATTGGAGTGGTAACGCGGGTAACTTAACAGCCGCCGGCGGCTGTTAAGTTACCCGCGTTACCACTCCAATCCAC	pPRP153	C107A
pPRP216	*prpF256*	GGATTGGAGTGGTAACAGCGGTAACTTAACAGCCGGCTGTTAAGTTACCGCTGTTACCACTCCAATCC	pPRP153	C107S
pPRP217	*prpF256*	GGATTGGAGTGGTAACAGCGGTAACTTAACAGCCGGCTGTTAAGTTACCGCTGTTACCACTCCAATCC	pPRP196	C107S
pPRP218	*prpF257*	CAACTTCTAGCACCAGCGCGACGGTTATACTGTCACGTGACAGTATAACCGTCGCGCTGGTGCTAGAAGTTG	pPRP153	K73A
pPRP219	*prpF258*	GCAACTTCTAGCACCAGCGAAACGGTTATACTGTCACACGTGTGACAGTATAACCGTTTCGCTGGTGCTAGAAGTTGC	pPRP153	K73E
pPRP220	*prpF257*	CAACTTCTAGCACCAGCGCGACGGTTATACTGTCACGTGACAGTATAACCGTCGCGCTGGTGCTAGAAGTTG	pPRP196	K73A
pPRP221	*prpF258*	GCAACTTCTAGCACCAGCGAAACGGTTATACTGTCACACGTGTGACAGTATAACCGTTTCGCTGGTGCTAGAAGTTGC	pPRP196	K73E
pPRP223	*prpF259*	CAACTTCTAGCACCAGCATGACGGTTATACTGTCACGTGACAGTATAACCGTCATGCTGGTGCTAGAAGTTG	pPRP153	K73M
pPRP225	*prpF255*	GTGGATTGGAGTGGTAACGCGGGTAACTTAACAGCCGCCGGCGGCTGTTAAGTTACCCGCGTTACCACTCCAATCCAC	pPRP196	C107A
pPRP226	*prpF259*	CAACTTCTAGCACCAGCATGACGGTTATACTGTCACGTGACAGTATAACCGTCATGCTGGTGCTAGAAGTTG	pPRP196	K73M

https://doi.org/10.1371/journal.pone.0188130.t002

overnight with isopropyl-ß-D-thiogalactopyranoside (IPTG, 0.3 mM) at an OD_{650} of ~0.8. Recombinant PrpD, apo-AcnA and apo-AcnB proteins from *S. enterica* were purified from *E. coli* as His-tagged proteins as described [15]. *So*AcnD protein was purified as follows. Plasmid pPRP205 (*S. oneidensis acnD*$^+$) was introduced into *E. coli* strain BL21 (λDE3) by electroporation selecting for ampicillin resistance on LB agar + ampicillin. Single colonies were used to inoculate 20 ml of LB + ampicillin; cultures were grown overnight at 37˚C. Overnight cultures were used to inoculate two liters of LB + ampicillin, and cells were grown at 37˚C until the culture reached an OD_{650} of ~0.7. At that point, expression of the plasmid-encoded *S. oneidensis acnD*$^+$ gene was induced by the addition of IPTG (0.3 mM) to the medium, followed by an 18-h incubation period at 37˚C. Cells were harvested by centrifugation at 8,000 x *g* at 4˚C in 1-liter bottles using a JLA-8.l rotor and a Beckman/Coulter Avanti™ J-20 XPI centrifuge. Cells were broken by sonication (10 min, 50% duty, 5 s pulses, maximal setting) with a 550 Sonic Dismembrator (Fisher Scientific). Cell debris was removed by centrifugation at 39,000 x *g* for 20 min in a Beckman JA 25.5 rotor. The supernatant was filtered through a 0.45 μm filter (Thermo Fisher Scientific). Protein was isolated using Ni-chelate affinity chromatography on Novagen's His Bind® Resin following the manufacturer's protocols.

Crystallization and structural determination of *So*PrpF^{K73E}

*So*PrpF^{K73E} was screened for initial crystallization conditions in a 144-condition sparse matrix screen developed in the Rayment laboratory (unpublished information). Single, diffraction quality crystals were grown by hanging drop vapor diffusion by mixing 2 μL of 28 mg/mL *So*PrpF^{K73E} in 2-amino-2-(hydroxymethyl)propane-1,3-diol hydrochloride buffer (Tris-HCl, 10 mM, pH 7.6) containing NaCl (50 mM) with 2 μL well solution containing 2-(*N*-morpholino)ethanesulfonic acid buffer (MES, 100 mM, pH 6.0) containing sodium malonate (136 mM), polyethylene glycol 4000 (PEG 4K, 15% w/v) at room temperature. Hanging droplets were nucleated after 24 h from an earlier spontaneous crystallization event using a cat's whisker. Crystals grew to approximate dimensions of 200 X 200 X 400 μm within 3 days. The crystals were transferred directly to a cryoprotecting solution that contained MES buffer (100 mM, pH 6.0), sodium malonate (136 mM), PEG 4K (30% w/v) and vitrified by rapid plunging into liquid nitrogen. *So*PrpF^{K73E} crystallized in the space group $P2_1$ with unit cell dimensions of a = 51.8 Å, b = 103.4 Å, c = 78.1 Å and two chains in the asymmetric unit.

X-ray diffraction data were collected on a Pilatus detector at SBC Beamline 19-ID (Advanced Photon Source, Argonne National Laboratory, Argonne, IL) The X-ray data were processed and scaled using the HKL-2000 program that integrates data collection, data reduction, phasing and model building [25]. Relevant X-ray diffraction data collection statistics are presented in Table 3. The previously determined model for *So*PrpF apo structure (PDB ID: 2PVZ) was used as the search model to solve the *So*PrpF^{K73E} apo structure via molecular replacement with the program Phaser [26]. Alternate cycles of manual model building and least squares refinement with the programs COOT [27] Refmac [28] and Phenix [29] reduced the R-factor to 16.5% for all X-ray data from 50–1.22 Å. Relevant refinement statistics are presented in Table 3.

Reactivation of aconitases

The Fe/S centers of *S. enterica* AcnA (hereafter *Se*AcnA), AcnB (hereafter *Se*AcnB), and *So*AcnD were reactivated using described protocols without modifications [30, 31]. All solutions used were freed of dissolved O_2 by degassing as described [32, 33].

Table 3. Data collection and refinement statistics.

Data collection	$PrpF^{K73E}$
Space group	$P2_1$
Unit-cell	*a* = 51.8
parameters (Å)	*b* = 103.4
	c = 78.1
	β = 104.47˚
Wavelength	0.979
resolution range (Å)	50–1.22(1.24–1.22)[a]
reflections: measured	2973055
reflections: unique	227930
Redundancy	13.0 (6.1)
Completeness (%)	96.5 (84.5)
average I/	49.5 (2.4)
Rsym [b] (%)	5.3 (67.1)
*R*work [c] (%)	16.4 (23.2)
*R*free (%)	18.4 (28.6)
no. protein atoms	5907
no. water molecules	1013
Wilson B-value ($Å^2$)	14.5
Average B factors ($Å^2$)	
PrpF monomer A	17.2 for 2956
PrpF monomer B	19.1 for 2923
Ligand	16.5 for 28
Solvent	29.2 for 1013
Ramachandran (%)	
Most favored	98.0
Additionally	2.0
allowed	
Generously	0.0
allowed	
Disallowed	0.0
rms deviations	
Bond Lengths (Å)	0.006
Bond angles (Å)	1.066
Chiral	

[a]Data in parentheses represent highest resolution shell.

[b]*R*sym = Σ/I(hkl)–I/ / Σ/I(hkl)/, where the average intensity *I* is taken over all symmetry equivalent measurements and $I_{(hkl)}$ is the measured intensity for a given reflection.

[c]*R*factor = Σ/F(obs)–F(calc)/ / Σ/F(obs)/, where *R*work refers to the *R*factor for the data utilized in the refinement and *R*free refers to the *R*factor for 5% of the data that were excluded from the refinement.

https://doi.org/10.1371/journal.pone.0188130.t003

High-performance liquid chromatography (HPLC)

Enzyme-dependent dehydration of citrate and 2-methylcitrate was performed in 1-ml reaction mixtures containing Tris-HCl buffer (90 mM, pH 8.0 at 25˚C), citrate or 2-MC (5 mM), and *So*AcnD (10 μg of reactivated protein) or *S. enterica* PrpD (hereafter *Se*PrpD, 13 μg). Reaction mixtures were incubated for 1.5 h at 37˚C. Reactions were stopped by the addition of 10 N H_2SO_4 to a final concentration of 5 mM. Particulate matter was removed from reaction

products by filtration using a Spin-X® centrifuge tube filter (Costar), and products were resolved by HPLC using a Beckman/Coulter chromatograph equipped with an Aminex® HPX-87H HPLC organic acid analysis column (BioRad) equilibrated and developed isocratically with H_2SO_4 (5 mM). Elution of compound off the column was detected by monitoring the absorbance at 210 nm.

Kinetic analysis of *S. enterica* aconitases

All reactions were performed in Tris-HCl buffer (50 mM, pH 8.0 at 25˚C) containing KCl (100 mM). Enzyme was incubated in buffer for 3–5 min before reactions were initiated by the addition of either *cis*-aconitate or 2-methy-*cis*-aconitate as substrate. Reactions were performed in triplicate, and their progress was monitored using a Perkin Elmer (Norwalk, CT) Lambda 40 UV/Vis Spectrometer at 240 nm; temperature in the cuvettes was maintained with a circulating water bath set at 37˚C. Data collection and analysis was performed with Perkin Elmer UV Kinlab software. An extinction coefficient of 3800 M^{-1} cm^{-1} was used for *cis*-aconitate [34], and 4690 M^{-1} cm^{-1} was calculated for the chemically synthesized 2-methyl-*cis*-aconitate. Kinetic curves were each repeated three times, with each substrate concentration tested in triplicate. The reported values are the median of all three experiments. Data did not deviate more than 15% from the median value.

In vivo assessment of activity associated with variant *So*PrpF proteins

Growth curves of *S. enterica* strains were performed in NCE medium supplemented with succinate (30 mM, pH 7.0 at 25˚C) or propionate (30 mM, pH 7.0 at 25˚C) as carbon and energy source. In both cases a low concentration of glycerol (1 mM) was added to accelerate the catabolism of succinate or propionate. Strains were grown overnight in LB medium supplemented with the appropriate antibiotic. Two microliters of an overnight culture were used to inoculate 198 μl of NCE medium in a 96-well microtiter plate. Growth was monitored using an EL808™ microplate reader (Bio-Tek Instruments) with the incubation chamber set at 37˚C. Absorbance readings were recorded every 15 min at 630 nm with 850 s of shaking between readings. All cultures were grown in triplicate. Growth curves were plotted using Prism v4.0 software (GraphPad Software).

In vitro assessment of activity associated with variant *So*PrpF proteins

To analyze the activity of *So*PrpF variants, the product of the *So*AcnD enzyme was synthesized as follows. Reactivated *So*AcnD was incubated overnight at 30˚C with 2-MC (1 mM) in Tris-HCl buffer (50 mM, pH 8.0) containing KCl (100 mM). *So*AcnD protein was removed from the mixture by the addition of His-Mag™ Agarose Beads (Novagen) resuspended in Tris-HCl buffer (50 mM, pH 8.0) containing KCl (100 mM). His-Mag™ beads were removed, and reaction mixtures were pooled. *So*PrpF protein (100 ng) was added to the reactions, samples were taken as a function of time, and were resolved by HPLC as described above.

Results

*So*AcnD and *Se*PrpD synthesize different methylaconitate isomers

We previously showed that *So*PrpF has isomerase activity that can convert *cis*-aconitate to *trans*-aconitate [19]. Given that *So*PrpF isomerase activity is needed to restore growth of a *S. enterica prpD* strain with propionate, we surmised that *Se*PrpD and *So*AcnD must synthesize two different methylaconitate isomers, and that *So*PrpF isomerizes the *So*AcnD product into

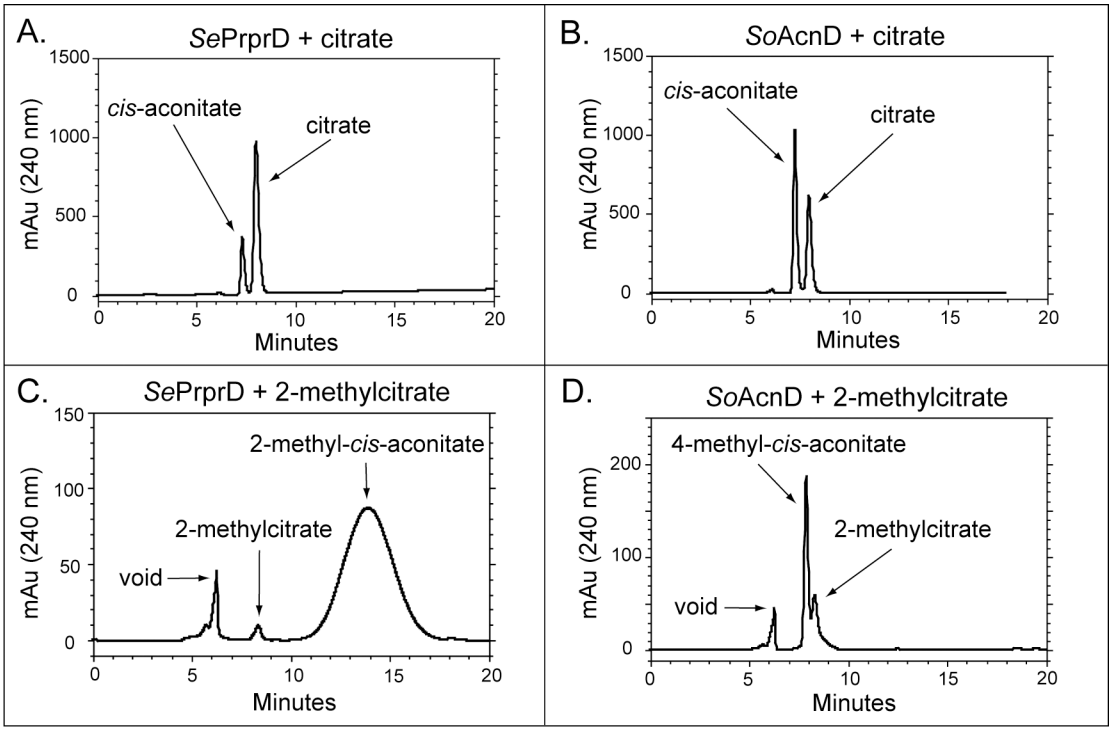

Fig 2. HPLC analysis of PrpD and AcnD reaction products. Reactions products when *Se*PrpD used citrate (panel A) or 2-methylcitrate (panel B) as substrate. Reaction products when *So*AcnD used citrate (panel B) or 2-methylcitrate (panel D) as substrate. Reaction mixtures were resolved by HPLC using a BioRad Aminex® HPX-87H Organic Acids Analysis column developed isocratically with 5 mM H_2SO_4 as the mobile phase. Elution was monitored at 240 nm.

https://doi.org/10.1371/journal.pone.0188130.g002

the *Se*PrpD product, so that *Se*AcnB, the next enzyme in the 2-MCC, can synthesize 2-methylisocitrate (Fig 1).

To test this hypothesis, we determined whether *Se*PrpD and *So*AcnD proteins synthesized different isomers of aconitate and methylaconitate. To do this, we incubated *Se*PrpD and *So*AcnD with citrate or 2-methylcitrate (each at 5 mM) in 1-ml reaction mixtures. After a 1.5-hr incubation period, the reactions mixtures were acidified with H_2SO_4 to a final concentration of 5 mM, and a 100 μl sample of the reaction was resolved by HPLC. When incubated with citrate, *Se*PrpD (Fig 2A) and *So*AcnD (Fig 2B) converted citrate (retention time ~8 min) into *cis*-aconitate (retention time ~7.2 min). When incubated with 2-methylcitrate, *Se*PrpD synthesized a product that eluted off the column as a broad peak centered at ~13.8 min (Fig 2C). On the other hand, *So*AcnD synthesized a product that eluted as a sharp peak at ~8 min (Fig 2D). The different retention times and chromatographic behavior indicated to us that the dehydration product of *Se*PrpD and *So*AcnD were different compounds. Analysis of chemically synthesized 2-methyl-*cis*-aconitate revealed a peak that matched the product of the *Se*PrpD reaction (Fig 2C), indicating that *Se*PrpD synthesized 2-methyl-*cis*-aconitate from 2-methylcitrate.

2-Methyl-*cis*-aconitate is a substrate of *Se*AcnA and *Se*AcnB

The HPLC chromatograms of the products of the *Se*PrpD and *So*AcnD reactions suggested that the *Se*PrpD product, 2-methyl-*cis*-aconitate, was the substrate that aconitases rehydrated to yield 2-methylisocitrate agreeing with previously reported data [35, 36]. Since *So*AcnD

cannot support growth with propionate in the absence of *So*PrpF, we surmised that the product of *So*AcnD was not a substrate of aconitases, but the product of the *So*PrpF reaction was.

Kinetic analysis of the *S. enterica* aconitases indicated that both, *Se*AcnA and *Se*AcnB, used 2-methyl-*cis*-aconitate as substrate to yield 2-methylisocitrate, albeit at a significantly slower rate than *cis*-aconitate, the TCA cycle intermediate (Table 4). The catalytic efficiencies of *Se*AcnA and *Se*AcnB were 40 and 60 lower when 2-methyl-*cis*-aconitate was the substrate than when *cis*-aconitate was the substrate, respectively. When 2-methyl-*cis*-aconitate ws the substrate, K_m values ranged from 180 to 229 μM and V_{max} values ranged from 50 to 60 μM min^{-1}. The numbers reported here are representative of three kinetic studies.

*So*PrpF isomerizes the *So*AcnD reaction product to 2-methyl-*cis*-aconitate

We tested whether *Se*AcnA and *Se*AcnB used the *So*AcnD reaction product as substrate (data not shown). The latter was synthesized from 2-MC using *So*AcnD. After the *So*AcnD enzyme was removed from the reaction mixture, either *Se*AcnA or *Se*AcnB was added, and the change in absorbance at 240 nm was monitored. Neither *Se*AcnA nor *Se*AcnB used the *So*AcnD reaction product as substrate. Purified *So*PrpF protein (100 μg) was added to the reaction mixture, and the reaction was allowed to proceed for one hour at 30˚C. Addition of *Se*AcnA resulted in specific activities of approximately 14 ± 1 nmol min^{-1} μg^{-1} of protein, while addition of *Se*AcnB resulted in specific activities of 48 ± 4 nmol min^{-1} μg^{-1} of protein. Additionally, HPLC analysis of the products of the *So*PrpF reactions indicated that *So*PrpF converted the *So*AcnD reaction product into 2-methyl-*cis*-aconitate over time (Fig 3), which can then be used as a substrate by the aconitase enzymes.

Analysis of variants to gain insights into the mechanism of *So*PrpF catalysis

Previous crystallographic data identified residues C107 and K73 in the active site of *So*PrpF as likely to be involved in catalysis. Residue C107 is formally equivalent to the catalytic base of diaminopimelate epimerase [19, 37, 38], and residue K73 is in a structurally equivalent position to the catalytic glutamate of the phenazine biosynthetic protein PhzF from *Pseudomonas fluorescens* [39]. We investigated the involvement of these two residues in *So*PrpF catalysis, using site-directed mutagenesis to introduce amino acids changes. Five *So*PrpF variants were constructed. Residue C107 was changed to either Ala or Ser, and residue K3 was changed to Ala, Glu, or Met. Plasmid pPRP153 (*prpF* in pBAD18-Kan) was used in *in vivo* complementation studies using a *S. enterica prpD* strain to assess the effect of specific substitutions on PrpF function. Substitutions at C107 (Fig 4A) and at K73 (Fig 4B) resulted in proteins that failed to

Table 4. Kinetics of AcnA and AcnB with *cis*-aconitate and 2-methyl-*cis*-aconitate.

Isomer/Enzyme used	K_m (μM)	V_{max} (μM min^{-1})	k_{cat} (min^{-1})	k_{cat} / K_m (min^{-1} μM^{-1})
***cis*-aconitate**				
AcnA	22 ± 2	86 ± 2	3739 ± 87	170
AcnB	17 ± 3	21 ± 1	2091 ± 100	123
2-methyl-*cis*-aconitate				
AcnA	210 ± 35	50 ± 3	708 ± 42	3.4
AcnB	208 ± 39	10 ± 1	396 ± 40	1.9

All kinetic reactions were performed in triplicate and individual kinetic curves were also repeated in triplicate. Reported values represent median values from all three experiments. No value differed more than 15% from the median value.

https://doi.org/10.1371/journal.pone.0188130.t004

support growth with propionate as a sole carbon and energy source in a *S. enterica* Δ*prpD* strain harboring a plasmid expressing *S. oneidensis acnD*$^+$. However, when growing on medium containing succinate and propionate (30 mM each), a much less stringent test for propionate utilization, both proteins with substitutions at C107 supported propionate catabolism (Fig 4C), albeit at a slower growth rate than the wild-type *prpF* allele, suggesting the presence of proteins with lower activity that could have been caused by misfolding. In contrast, none of the variants with substitutions at residue K73 supported growth under either condition (Fig 4D) suggestive of proteins that either lacked catalytic activity or were misfolded. We note that when grown on medium containing both succinate and propionate, the final cell density of the cultures was approximately 1.3–1.5 A_{630} units, which was substantially higher than the final density of approximately 1.0 A_{630} unit when growing with propionate alone, suggesting that the strains containing the mutant alleles encoding *So*PrpF variants used propionate and succinate as carbon and energy sources.

To assess the residual level of isomerase activity associated with variant *So*PrpF variants, appropriate mutations were introduced into plasmid pPRP196 (*prpF*$^+$ in pTEV4); proteins containing the C107A or K73A substitutions were not overproduced and could not be purified. The remaining variants were isolated, and their activity was quantified. None of the variants had any detectable activity. While this may be expected for substitutions of K73, the proposed catalytic residue, it is unclear why the C107S mutant had no activity, especially since the variants were active *in vivo*. More studies may need to be undertaken to fully understand this result.

Analysis of the tertiary and quaternary structures of the catalytically inactive *So*PrpF^{K73E} variant

To further understand the roles of residues K73 and C107, we solved the three-dimensional crystal structure of Apo-*So*PrpF^{K73E}, which crystallized in space group $P2_1$ with cell dimensions

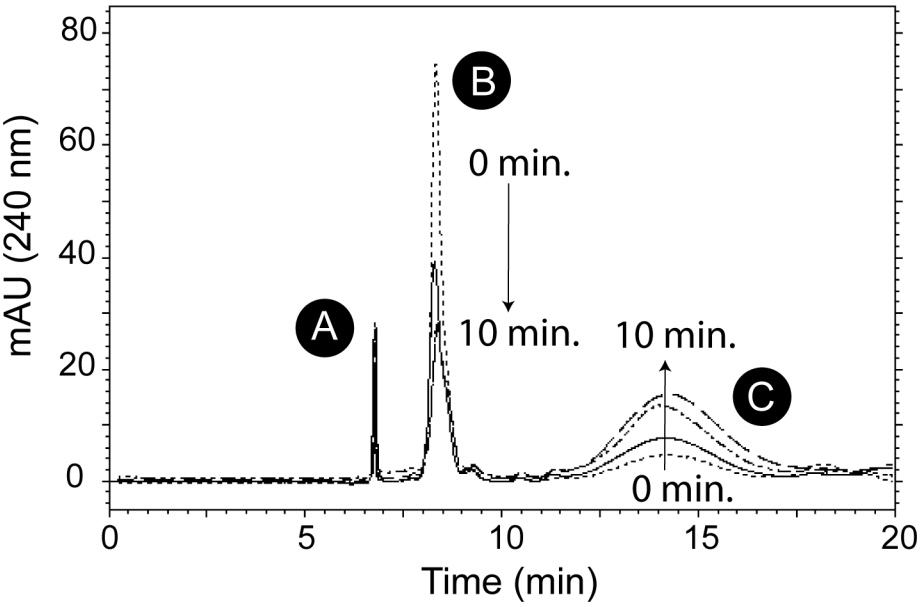

Fig 3. *So*PrpF isomerizes the *So*AcnD product into 2-methyl-*cis*-aconitate. Reactivated *So*AcnD was incubated with 2-MC, once *So*AcnD was removed from the reaction, PrpF was added (100 μg) and samples were removed at the indicated times stopped by the addition of H_2SO_4 to 5 mM. Reactions were resolved by HPLC using an Aminex HPX-87H Organic Acid column equilibrated and isocratically developed with 5 mM H_2SO_4; reaction products were monitored at 240 nm. A. void; B. 4-methyl-*cis*-aconitate C. 2-methyl-*cis*-aconitate.

https://doi.org/10.1371/journal.pone.0188130.g003

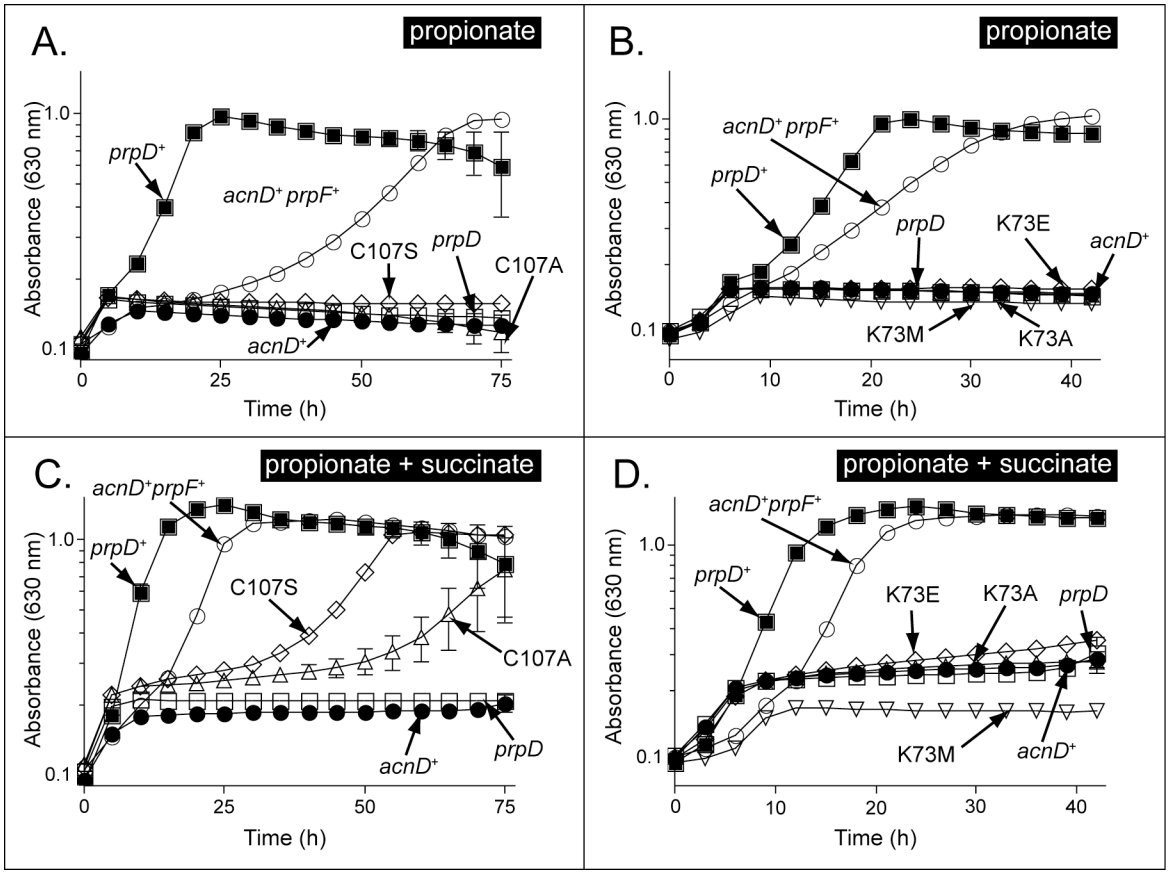

Fig 4. Growth behavior analysis of strains synthesizing variants of PrpF. Growth curves were performed in NCE minimal medium supplemented with propionate (30 mM) (Panels A, B) or propionate + succinate (30 mM ea.) (Panels C, D). Plasmids encoding PrpF variants with substitutions at position C107 failed to restore growth of strains JE9373 (*prpD* / pAcnD^{WT} pPrpF^{C107A}) or JE9374 (*prpD* pAcnD^{WT} pPrpF^{C107S}) with propionate (Panel A: PrpF^{C107S}, open diamonds; PrpF^{C107A}, open triangles, respectively), but did restore growth with propionate + succinate, albeit at a slower rate (panel C, diamonds, triangles, respectively). In contrast, substitutions at position K73 failed to compensate for the absence of PrpD on either propionate (panel B: PrpF^{K73A}, open triangles; PrpF^{K73E}, open diamonds, PrpF^{K73M}, open inverted triangles), or succinate + propionate (Panel D: PrpF^{K73A}, open triangles; PrpF^{K73E}, open diamonds; PrpF^{K73M}, open inverted triangles).

https://doi.org/10.1371/journal.pone.0188130.g004

a = 51.8 b = 103.4 c = 78.1 Å, and contained two monomers per asymmetric unit. The structure was determined at 1.22Å resolution by molecular replacement using apo-*So*PrpF (PDB ID: 2PVZ) as a search model (Table 3). The two monomers in the asymmetric unit are related by a non-crystallographic twofold axis. The two monomers are highly similar where the rms difference between 381 α-carbon atoms is 0.13Å. Given the similarity between the two monomers, all of the discussion of the structure of a single protein chain is based on that of subunit A.

*So*PrpF assembles to form a homodimer and buries 2400Å^2 of surface area per monomer, which represents 15% of each monomer's total surface area (Fig 5A). While the *So*PrpF^{K73E} variant structure can be superposed closely with both the apo-PrpF^{W}T and *trans*-aconitate bound structures with rms differences of 0.6 Å and 0.4 Å over 385 α-carbon respectively, an alignment of the N-terminal domains from residues 5–185 reveals that the C-terminal domain of the *So*PrpF^{K73E} structure rotates into a more open conformation. The C-terminal domain rotates ~4.4˚ between the extremes provided by the apo (closed) and aconitate (open) bound forms. This rotation occurs around the segments that connect the N-terminal and C-terminal domain (E180-N183 and I379-M380) although there are negligible conformational changes

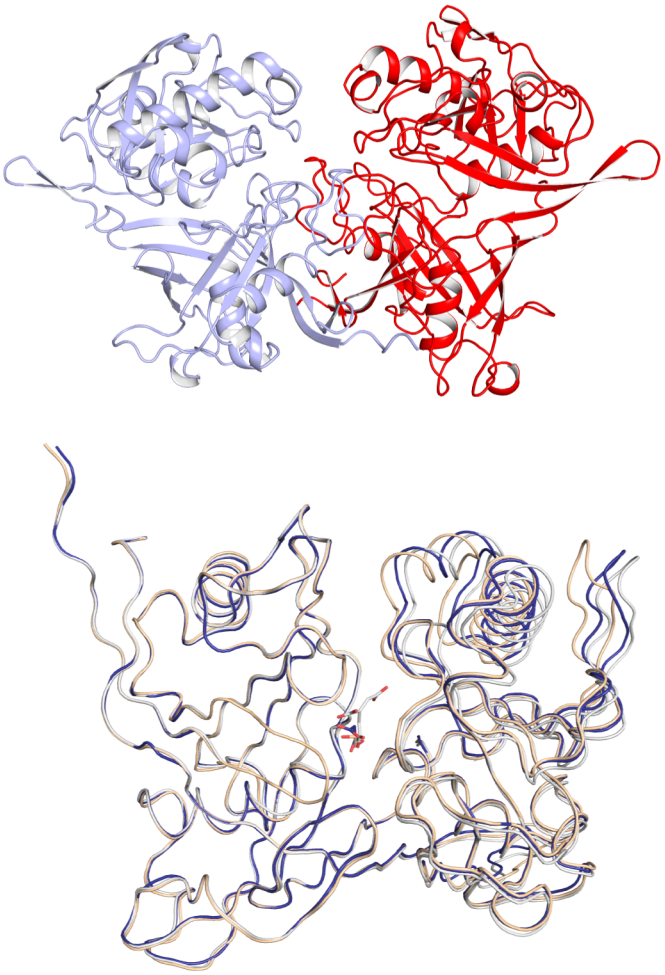

Fig 5. Crystal structure of *So*PrpF^{K73E} at 2.35Å resolution. A. Ribbon representation of the *So*PrpF^{K73E} homodimer (*light blue* = monomer A, *red* = monomer B). **B.** Overlay of *So*PrpF^{K73E} (*blue)*, *So*PrpF in complex with *trans*-aconitate (*white*, RCSB accession number 2PW0) and apo-*So*PrpF^{WT} (*tan*, RCSB accession number 2PVZ). The superposition was performed by aligning residues 1–185 with the program Superpose [40]. Figs 5 and 6 were prepared with the program Pymol; DeLano Scientific LLC, Palo Alto, CA.

https://doi.org/10.1371/journal.pone.0188130.g005

associated with these residues since they represent the fulcrum point for the rotation. As such these residues cannot be viewed as a flexible hinge.

A comparison of the three structures showed that the *trans*-aconitate bound structure was in the most open conformation, while the *So*PrpF^{K73E} structure was intermediate and the apo-*So*PrpF^{WT} structure was in the most closed conformation (Fig 5B). This was not surprising as a glycerol molecule, derived from the cryoprotectant used in the structural determination, was bound in the active site of the apo-*So*PrpF^{WT} structure. Glycerol is a smaller ligand than the true substrate and thus allows the C-terminal domain to move closer to the N-terminal domain since it is not impeded by the larger *trans*-aconitate molecule. Similarly, a malonate molecule derived from the crystallization solution was bound in the active site of the *So*PrpF^{K73E} structure. Because malonate is larger than glycerol and smaller than *trans*-aconitate, the C-terminal domain adopted an intermediary conformation. Thus, the structure of the apo-*So*PrpF^{K73E} variant protein provided an estimate of the conformational freedom available to the N- and C-terminal domains of PrpF. Attempts to obtain substrate complexed

*So*PrpF^{K73E} crystals by co-crystallization or soaking into apo crystals with either *trans*-aconitate or 2-methylcitrate were not successful. This difficulty in co-crystallization was not surprising since binding of *trans*-aconitate into the *So*PrpF^{K73E} active site would position a substrate carboxyl moiety within 3 Å of the new glutamate carboxyl group of *So*PrpF^{K73E} variant, thus creating an unfavorable interaction (Fig 6).

Phylogenetic analysis of PrpF homologues

To provide some perspective of the wide distribution of PrpF homologues in nature, we performed a limited phylogenetic analysis of 70 microbes containing a total of 86 PrpF homologues using the MUltiple Sequence Comparison by Log-Expectation (MUSCLE) software. For this purpose, one hundred sequences were selected and aligned (Fig 7). Proteins displaying the shortest distances from the root (clusters at the top and bottom of the tree, respectively) were mostly found in operons with genes related to propionate catabolism. Proteins that are more divergent were more likely to be found in alternate genetic contexts. In Fig 7, proteins from Gram-positive species are indicated with squares and proteins from fungi are indicated with circles. When an organism possesses multiple copies of the gene, the additional copies that are not found to be associated with propionate catabolic genes are marked with triangles. As can be noted in the tree, proteins found in organisms that are more distant evolutionarily from the Gamma-proteobacteria, and proteins not involved in propionate catabolism tend to be more distant in the phylogenetic tree as well.

Discussion

In this paper, we show that the PrpF protein of *S*. *oneidensis* (*So*PrpF) has isomerase activity that converts the product of the *So*AcnD reaction into 2-methyl-*cis*-aconitate, which can then be converted into 2-methylisocitrate by aconitase. The *So*AcnD product is likely 4-methyl-*cis*-aconitate. On the basis of the analysis of the crystal structures of *So*PrpF^{WT} and *So*PrpF^{K73E}, we propose that *So*AcnD dehydrates 2-methylcitrate into 4-methyl-*cis*-aconitate. We established the order of the 2-MCC in *Shewanella oneidensis* and, by inference, in other bacteria that contain *acnD* and *prpF* homologues in their *prp* operons. That is, in organisms that use the AcnD/PrpF enzymes instead of PrpD, 2-methylcitrate is dehydrated by AcnD to 4-methyl-*cis*-aconitate, which is then isomerized to 2-methyl-*cis*-aconitate by PrpF, and rehydrated to 2-methylisocitrate by aconitases (Fig 1).

Rationale for the use of the AcnD/PrpF system

It is unclear why some bacteria such as *S*. *oneidensis* and *V*. *cholera* use AcnD and PrpF to synthesize 2-methyl-*cis*-aconitate, while others use a PrpD homologue. This work does not address this interesting question, but it does provide experimental data to support the assignment of a biochemical activity for the *So*PrpF enzyme.

We note that a previous report suggested that the formation of 2-methyl-*cis*-aconitate must occur via a unique *syn* elimination of water [3]. To date, a detailed analysis of the mechanism of *So*AcnD or any of its homologues has not been reported. Thus, for the sake of this discussion, we will assume that the *So*AcnD protein, like most aconitases, is limited to *anti* β-eliminations [41]. Therefore, like other aconitases, *So*AcnD would remove the *pro-R* proton from the oxaloacetate-derived carbon of citrate (C-4), not from the carbon derived from acetate (C-2) [42]. In 2-methylcitrate, carbons 3, 4, and 5 are the carbons derived from oxaloacetate, and as such, carbons 3 and 4 should be where *So*AcnD dehydrates the substrate. The C2 of 2-methylcitrate is derived from propionate, and should not participate in the *So*AcnD-catalyzed

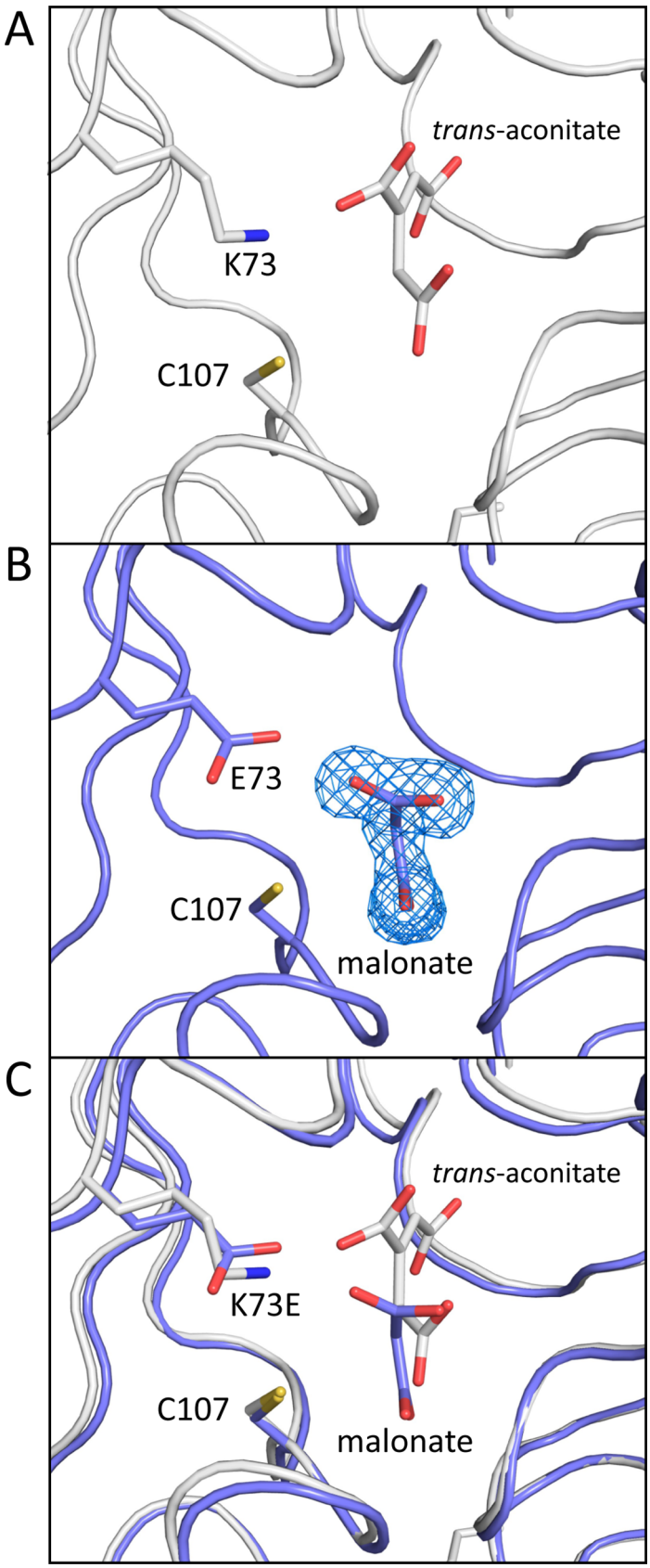
A
trans-aconitate
K73
C107
B
E73
C107
malonate
C
trans-aconitate
K73E
C107
malonate

Fig 6. Active site comparisons of *So*PrpF^{WT} and *So*PrpF^{K73E}. A. Detailed view of the catalytic active site residues, which contact *trans*-aconitate in the *So*PrpF^{WT} protein determined in the presence of *trans*-aconitate (RCSB accession number 2pw0). **B.** Detailed view of the residues lining the active site in the *So*PrpF^{K73E} variant with malonate bound. The electron density map was calculated with coefficients of the form F_o-F_c where the ligand was omitted from the final phase calculation refinement and contoured to 4.5 σ. **C.** The superposition of active site residues with *trans*-aconitate and malonate included for reference.

https://doi.org/10.1371/journal.pone.0188130.g006

dehydration reaction. An *anti* ß-elimination of the *pro-R* proton at C4 should result specifically in the formation of 4-methyl-*cis*-aconitate by *Se*AcnD.

Since *So*AcnD is likely to yield 4-methyl-*cis*-aconitate, the presence of an isomerase, like *So*PrpF, becomes necessary, as the accumulation of 4-methyl-*cis*-aconitate could inhibit aconitase. Isomerization of 4-methyl-*cis*-aconitate to 2-methyl-*cis*-aconitate then allows aconitase to convert the latter to 2-methylisocitrate, which is cleaved by the 2-methylisocitrate lyase yielding succinate and pyruvate (Fig 1). The greater activity of *Se*AcnB on enzymatically-derived 2-methyl-*cis*-aconitate when compared to *Se*AcnA suggests AcnB is the primary aconitase utilized in propionate catabolism, which is in agreement with our previously reported data that indicated *Se*AcnB was the primary aconitase involved in propionate catabolism [15].

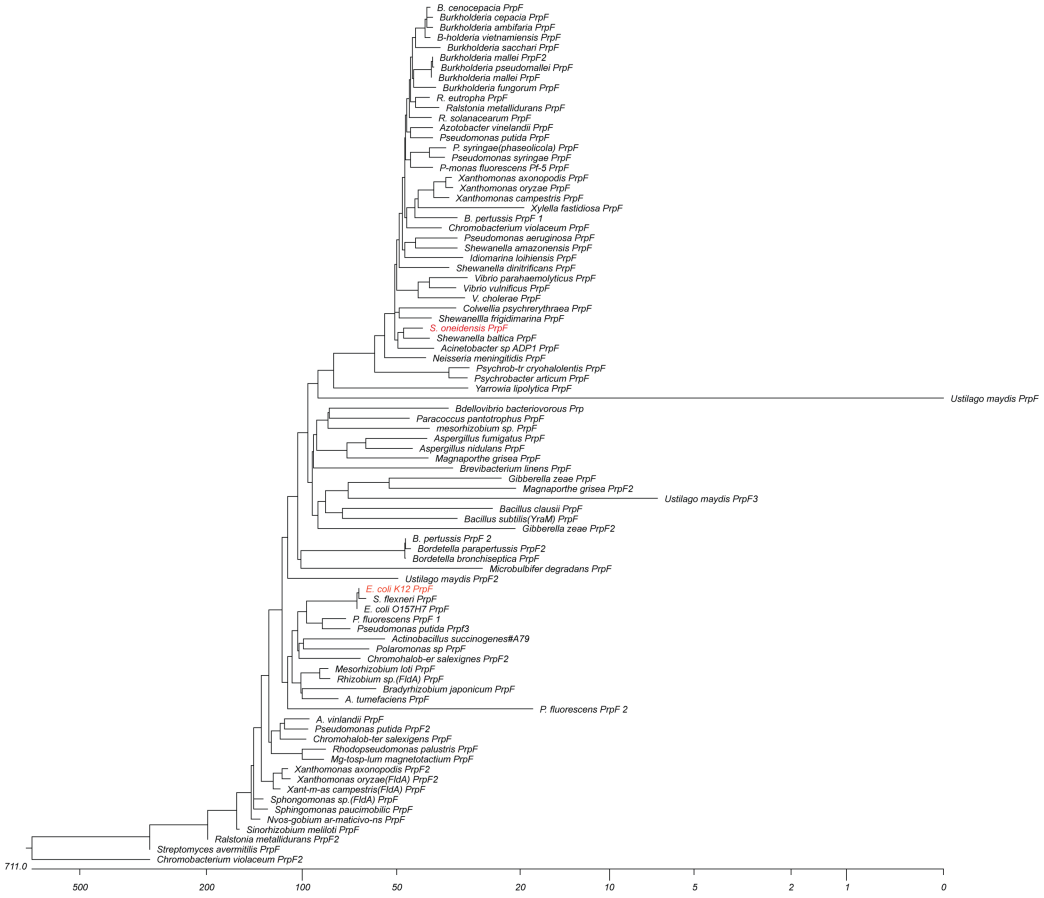

Fig 7. Phylogenetic tree of selected PrpF homologues in nature. Phylogenetic tree of selected PrpF homologues. Eighty-six sequences were selected and aligned using ClustalW software. Proteins towards the top of the tree are mostly found in operons with genes related to propionate catabolism. Proteins that are more divergent are more likely to be found in alternate genetic contexts. The PrpF protein of *Shewanella oneidensis* and the *E. coli* K12 PrpF homologue are highlighted in red. Distance is shown in substitutions per 100 residues.

https://doi.org/10.1371/journal.pone.0188130.g007

Modifications to the 2-methylcitric acid cycle

The identification of *So*PrpF as a 4-methyl-*cis*-aconitate isomerase resolves the issue of why *So*AcnD and *So*PrpF proteins are required to restore propionate catabolism in a Δ*prpD* strain in *S. enterica* (18). Fig 1 reflects the findings of this work, in that it shows the sequence of reactions catalyzed by AcnD and PrpF.

Why AcnD, and not any of the other aconitases?

It is unclear why any organism would dedicate an aconitase to the 2-MCC, given that several aconitases already exist in the cell. Studies of the conformation of mitochondrial aconitases suggest that the methyl group of 2-methylcitrate may sterically interfere with this compound entering the active site correctly [43]. We suggest that the active site of *So*AcnD may be different enough to use 2-methylcitrate as a substrate.

Structure-function analysis of the *So*PrpF active site

In our previous work we suggested that active site of PrpF utilized a single catalytic lysine (Lys 73) to catalyze a proton extraction and a conformational rearrangement around the C2-C3 bond [19]. Data presented here indicates that the reaction instead involves an allylic rearrangement and bond migration mechanism of an aconitate isomerase from *Pseudomonas putida* described by Klinman and Rose that may have been a PrpF homologue [44]. However, using an allylic rearrangement mechanism would require two catalytic residues and PrpF appears to only have one. The most likely candidate for a second catalytic residue would be C107, which is formally equivalent to the catalytic residue of diaminopimelate epimerase. A recent publication suggested that 4-methyl-*cis*-aconitate would bind in a manner that would allow the C107 to function as a second catalytic residue [45]. Our mutational analysis sheds light on this possibility. If C107 were required for function, complete loss of enzyme activity in variants with substitutions in C107 would be expected. In Fig 4A, we present *in vivo* evidence in support for a critical role for C107. When propionate was used as the sole source of carbon and energy, the *So*PrpF$^{C107S/A}$ variants failed to support growth of a Δ*prpD* strain expressing *So*AcnD. Although *So*PrpF$^{C107S/A}$ variants retain activity (Fig 4C), it is insufficient to support growth with propionate as a carbon and energy source. Further work is needed to better understand the catalytic mechanism of *So*PrpF.

Significance of the broad distribution of PrpF homologues

The widespread distribution of genes encoding PrpF homologues in prokaryotes and eukaryotes, reveals the importance of isomerization in cell physiology. While the majority of the bacterial homologues appear to be part of operons along with other propionate utilization genes, many of them are present in operons encoding genes of unknown function. These *prpF* homologues suggest the possibility of double-bond isomerization being involved in many metabolic pathways.

In summary, we report data in support the following conclusions: i) PrpF isomerizes 4-methyl-*cis*-aconitate into 2-methyl-*cis*-aconitate; ii) the product of the AcnD reaction with 2-methylcitrate is most likely 4-methyl-*cis*-aconitate; iii) the aconitase proteins of *S. enterica* (*i. e.*, AcnA, AcnB) only rehydrate 2-methyl-*cis*-aconitate to 2-methylisocitrate; and iv) the proposed catalytic lysine (Lys 73) is absolutely required for activity of PrpF, and while substitutions of C107 do not abolish enzyme activity, PrpF^{C107} variants do not support growth with propionate.

Conclusions

Work reported in this paper advances our understanding of the 2-methylcitric acid cycle responsible for the conversion of the short-chain fatty acid propionate to pyruvate. The best-characterized sequence of reactions of the pathway involves the PrpD enzyme, which dehydrates 2-methylcitrate to 2-methyl-*cis*-aconitate. However, some microorganisms have replaced PrpD with two proteins, namely AcnD and PrpF, whose functions are not well understood. *In vivo* and *in vitro* evidence presented in this paper support to the conclusion that in an AcnD/PprF-dependent 2-methylcitric acid cycle, AcnD likely generates 4-methyl-*cis*-aconitate, which is isomerized by PrpF into 2-methyl-*cis*-aconitate. Additional work is needed to confirm the identity of the *So*AcnD product. Structural analysis of an inactive variant of PrpF provides insights into its mechanism of function. A better understanding of PrpF activity will be of value to other investigators researching the function of PrpF-like isomerases, which are widely distributed among prokaryotes.

Supporting information

S1 Fig. Kinetics of aconitase product formation. Reaction mixtures contained aconitase A (AcnA) and aconitase B (AcnB) with *cis*-aconitate (Panel A: AcnA; Panel B: AcnB) or 2-methyl-*cis*-aconitate (Panel C: AcnA; Panel D: AcnB) as substrate. Product formation (either isocitrate from *cis*-aconitate; 2-methylisocitrate from 2-methy-*cis*-aconitate) was monitored as a decrease in absorbance at 240 nm over time (min; *y*-axes) as a function of substrate concentration (μM; *x* axes). The increase in the rate at which A_{240} decreased is what is plotted. Detailed assay conditions are described under *Materials and methods*.
(PDF)

Acknowledgments

The authors do not have any conflict of interest to declare. The atomic coordinates and structure factors for $SoPrpF^{K73E}$ have been deposited in the Protein Data Bank, Research Collaboratory for Structural Bioinformatics, Rutgers University, New Brunswick, NJ (http://www.rcsb.org/) with accession code 5K87.

Author Contributions

Conceptualization: Christopher J. Rocco, Karl M. Wetterhorn, Ivan Rayment, Jorge C. Escalante-Semerena.

Data curation: Christopher J. Rocco, Karl M. Wetterhorn, Graeme S. Garvey, Ivan Rayment, Jorge C. Escalante-Semerena.

Formal analysis: Christopher J. Rocco, Karl M. Wetterhorn, Graeme S. Garvey, Ivan Rayment, Jorge C. Escalante-Semerena.

Funding acquisition: Ivan Rayment, Jorge C. Escalante-Semerena.

Investigation: Christopher J. Rocco, Karl M. Wetterhorn, Graeme S. Garvey.

Methodology: Christopher J. Rocco.

Project administration: Jorge C. Escalante-Semerena.

Supervision: Ivan Rayment, Jorge C. Escalante-Semerena.

Validation: Christopher J. Rocco, Karl M. Wetterhorn, Graeme S. Garvey.

Writing – original draft: Christopher J. Rocco, Karl M. Wetterhorn, Graeme S. Garvey, Ivan Rayment, Jorge C. Escalante-Semerena.

Writing – review & editing: Christopher J. Rocco, Ivan Rayment, Jorge C. Escalante-Semerena.

References

1. Tabuchi T, Hara S. Production of 2-methylcitric acid from n-parafins by mutants of Candida lipolytica. Agr Biol Chem. 1974; 38:1105–6.
2. Horswill AR, Escalante-Semerena JC. *Salmonella typhimurium* LT2 catabolizes propionate via the 2-methylcitric acid cycle. J Bacteriol. 1999; 181:5615–23. PMID: 10482501
3. Brock M, Maerker C, Schutz A, Völker U, Buckel W. Oxidation of propionate to pyruvate in *Escherichia coli*. Involvement of methylcitrate dehydratase and aconitase. Eur J Biochem. 2002; 269:6184–94. PMID: 12473114
4. Textor S, Wendisch VF, De Graaf AA, Muller U, Linder MI, Linder D, et al. Propionate oxidation in Escherichia coli: evidence for operation of a methylcitrate cycle in bacteria. Arch Microbiol. 1997; 168:428–36. PMID: 9325432
5. Munoz-Elias EJ, Upton AM, Cherian J, McKinney JD. Role of the methylcitrate cycle in *Mycobacterium tuberculosis* metabolism, intracellular growth, and virulence. Mol Microbiol. 2006; 60:1109–22. https://doi.org/10.1111/j.1365-2958.2006.05155.x PMID: 16689789
6. Upton AM, McKinney JD. Role of the methylcitrate cycle in propionate metabolism and detoxification in *Mycobacterium smegmatis*. Microbiology. 2007; 153:3973–82. https://doi.org/10.1099/mic.0.2007/011726-0 PMID: 18048912
7. Savvi S, Warner DF, Kana BD, McKinney JD, Mizrahi V, Dawes SS. Functional characterization of a vitamin B_{12}-dependent methylmalonyl pathway in *Mycobacterium tuberculosis*: implications for propionate metabolism during growth on fatty acids. J Bacteriol. 2008; 190:3886–95. https://doi.org/10.1128/JB.01767-07 PMID: 18375549
8. Huser AT, Becker A, Brune I, Dondrup M, Kalinowski J, Plassmeier J, et al. Development of a *Corynebacterium glutamicum* DNA microarray and validation by genome-wide expression profiling during growth with propionate as carbon source. J Biotechnol. 2003; 106:269–86. PMID: 14651867
9. Claes WA, Puhler A, Kalinowski J. Identification of two *prpDBC* gene clusters in *Corynebacterium glutamicum* and their involvement in propionate degradation via the 2-methylcitrate cycle. J Bacteriol. 2002; 184:2728–39. https://doi.org/10.1128/JB.184.10.2728-2739.2002 PMID: 11976302
10. Brämer CO, Steinbüchel A. The methylcitric acid pathway in *Ralstonia eutropha*: new genes identified involved in propionate metabolism. Microbiology. 2001; 147:2203–14. https://doi.org/10.1099/00221287-147-8-2203 PMID: 11495997
11. Brämer CO, Silva LF, Gomez JG, Priefert H, Steinbüchel A. Identification of the 2-methylcitrate pathway involved in the catabolism of propionate in the polyhydroxyalkanoate-producing strain *Burkholderia sacchari* IPT101(T) and analysis of a mutant accumulating a copolyester with higher 3-hydroxyvalerate content. Appl Environ Microbiol. 2002; 68:271–9. https://doi.org/10.1128/AEM.68.1.271-279.2002 PMID: 11772636
12. Horswill AR, Escalante-Semerena JC. Propionate catabolism in *Salmonella typhimurium* LT2: two divergently transcribed units comprise the *prp* locus at 8.5 centisomes, *prpR* encodes a member of the sigma-54 family of activators, and the *prpBCDE* genes constitute an operon. J Bacteriol. 1997; 179:928–40. PMID: 9006051
13. Grimek TL, Holden H, Rayment I, Escalante-Semerena JC. Residues C123 and D58 of the 2-methylisocitrate lyase (PrpB) enzyme of *Salmonella enterica* are essential for catalysis. J Bacteriol. 2003; 185:4837–43. https://doi.org/10.1128/JB.185.16.4837-4843.2003 PMID: 12897003
14. Grimm C, Evers A, Brock M, Maerker C, Klebe G, Buckel W, et al. Crystal structure of 2-methylisocitrate lyase (PrpB) from *Escherichia coli* and modelling of its ligand bound active centre. J Mol Biol. 2003; 328:609–21. PMID: 12706720
15. Horswill AR, Escalante-Semerena JC. In vitro conversion of propionate to pyruvate by *Salmonella enterica* enzymes: 2-methylcitrate dehydratase (PrpD) and aconitase enzymes catalyze the conversion of 2-methylcitrate to 2-methylisocitrate. Biochemistry. 2001; 40:4703–13. PMID: 11294638
16. Horswill AR, Escalante-Semerena JC. The *prpE* gene of *Salmonella typhimurium* LT2 encodes propionyl-CoA synthetase. Microbiology. 1999; 145:1381–8. https://doi.org/10.1099/13500872-145-6-1381 PMID: 10411265

17. Horswill AR, Escalante-Semerena JC. Characterization of the propionyl-CoA synthetase (PrpE) enzyme of *Salmonella enterica*: Residue Lys592 is required for propionyl-AMP synthesis. Biochemistry. 2002; 41:2379–87. PMID: 11841231

18. Grimek TL, Escalante-Semerena JC. The *acnD* genes of *Shewenella oneidensis* and *Vibrio cholerae* encode a new Fe/S-dependent 2-methylcitrate dehydratase enzyme that requires *prpF* function in vivo. J Bacteriol. 2004; 186:454–62. https://doi.org/10.1128/JB.186.2.454-462.2004 PMID: 14702315

19. Garvey GS, Rocco CJ, Escalante-Semerena JC, Rayment I. The three-dimensional crystal structure of the PrpF protein of *Shewanella oneidensis* complexed with trans-aconitate: Insights into its biological function. Protein Sci. 2007; 16:1274–84. https://doi.org/10.1110/ps.072801907 PMID: 17567742

20. Bertani G. Studies on lysogenesis. I. The mode of phage liberation by lysogenic *Escherichia coli*. J Bacteriol. 1951; 62:293–300. PMID: 14888646

21. Bertani G. Lysogeny at mid-twentieth century: P1, P2, and other experimental systems. J Bacteriol. 2004; 186:595–600. https://doi.org/10.1128/JB.186.3.595-600.2004 PMID: 14729683

22. Berkowitz D, Hushon JM, Whitfield HJ Jr., Roth J, Ames BN. Procedure for identifying nonsense mutations. J Bacteriol. 1968; 96:215–20. PMID: 4874308

23. Davis RW, Botstein D, Roth JR. A manual for genetic engineering: advanced bacterial genetics. Cold Spring Harbor, NY: Cold Spring Harbor Laboratory Press; 1980.

24. Rocco CJ, Dennison KL, Klenchin VA, Rayment I, Escalante-Semerena JC. Construction and use of new cloning vectors for the rapid isolation of recombinant proteins from *Escherichia coli*. Plasmid. 2008; 59:231–7. https://doi.org/10.1016/j.plasmid.2008.01.001 PMID: 18295882

25. Otwinowski Z, Minor W. Processing of X-ray diffraction data collected in oscillation mode. Methods Enzymol. 1997; 276:307–26.

26. McCoy AJ, Grosse-Kunstleve RW, Adams PD, Winn MD, Storoni LC, Read RJ. Phaser crystallographic software. J Appl Crystallogr. 2007; 40:658–74. https://doi.org/10.1107/S0021889807021206 PMID: 19461840

27. Emsley P, Cowtan K. Coot: model-building tools for molecular graphics. Acta Crystallogr D Biol Crystallogr. 2004; 60:2126–32. https://doi.org/10.1107/S0907444904019158 PMID: 15572765

28. Murshudov GN, Vagin AA, Dodson EJ. Refinement of macromolecular structures by the Maximum-Likelihood Method. Acta Crystallogr D Biol Crystallogr. 1997; 53:240–55. https://doi.org/10.1107/S0907444996012255 PMID: 15299926

29. Adams PD, Afonine PV, Bunkoczi G, Chen VB, Davis IW, Echols N, et al. PHENIX: a comprehensive Python-based system for macromolecular structure solution. Acta Crystallogr D Biol Crystallogr. 2010; 66:213–21. https://doi.org/10.1107/S0907444909052925 PMID: 20124702

30. Kennedy MC, Spoto G, Emptage MH, Beinert H. The active site sulfhydryl of aconitase is not required for catalytic activity. J Biol Chem. 1988; 263(17):8190–3. PMID: 2836416

31. Kennedy MC, Beinert H. The state of cluster SH and S2- of aconitase during cluster interconversions and removal. A convenient preparation of apoenzyme. J Biol Chem. 1988; 263:8194–8. PMID: 2836417

32. Gunsalus RP, Tandon SM, Wolfe RS. A procedure for anaerobic column chromatography employing an anaerobic Freter-type chamber. Anal Biochem. 1980; 101(2):327–31. PMID: 7362029

33. Balch WE, Wolfe RS. New approach to the cultivation of methanogenic bacteria: 2-mercaptoethanesulfonic acid (HS-CoM)-dependent growth of *Methanobacterium ruminantium* in a pressurized atmosphere. Appl Environ Microbiol. 1976; 32:781–91. PMID: 827241

34. Kennedy MC, Emptage MH, Dreyer JL, Beinert H. The role of iron in the activation-inactivation of aconitase. J Biol Chem. 1983; 258:11098–105. PMID: 6309829

35. Schloss JV, Emptage MH, Cleland WW. pH Profiles and isotope effects for aconitases from *Saccharomycopsis ipolytica*, beef heart, and beef liver—Alpha-methyl-*cis*-aconitate and *threo*-Ds-alpha-methylisocitrate as substrates. Biochemistry. 1984; 23:4572–80. PMID: 6093859

36. Aoki H, Uchiyama H, Umetsu H, Tabuchi T. Isolation of 2-methylisocitrate dehydratase, a new Eenzyme serving in the methylcitric acid cycle for propionate metabolism, from *Yallowia lipolytica*. Biosci Biotech Biochem. 1995; 59:1825–8.

37. Cirilli M, Zheng R, Scapin G, Blanchard JS. Structural symmetry: the three-dimensional structure of *Haemophilus influenzae* diaminopimelate epimerase. Biochemistry. 1998; 37:16452–8. https://doi.org/10.1021/bi982138o PMID: 9843410

38. Koo HM, Kim YS. Identification of active-site residues in *Bradyrhizobium japonicum* malonyl-coenzyme A synthetase. Arch Biochem Biophys. 2000; 378:167–74. https://doi.org/10.1006/abbi.2000.1813 PMID: 10871057

39. Blankenfeldt W, Kuzin AP, Skarina T, Korniyenko Y, Tong L, Bayer P, et al. Structure and function of the phenazine biosynthetic protein PhzF from *Pseudomonas fluorescens*. Proc Natl Acad Sci U S A. 2004; 101:16431–6. https://doi.org/10.1073/pnas.0407371101 PMID: 15545603

40. Krissinel E, Henrick K. Secondary-structure matching (SSM), a new tool for fast protein structure alignment in three dimensions. Acta Crystalogr Sec D Biol Crystalogr. 2004; D60:2256–68.

41. Hanson KR, Rose IA. The absolute stereochemical course of citric acid biosynthesis. Proc Natl Acad Sci U S A. 1963; 50:981–8. PMID: 14082366

42. Gawron O, Glaid AJ, Fondy TP, Bechtold MM. Stereochemistry of the succinic dehydrogenase system. Nature. 1961; 189:1004–5. PMID: 13704063

43. Lauble H, Stout CD. Steric and conformational features of the aconitase mechanism. Proteins. 1995; 22 (1):1–11. https://doi.org/10.1002/prot.340220102 PMID: 7675781

44. Klinman JP, Rose IA. Mechanism of the aconitate isomerase reaction. Biochemistry. 1971; 10:2259–66. PMID: 5114988

45. Velarde M, Macieira S, Hilberg M, Broker G, Tu SM, Golding BT, et al. Crystal structure and putative mechanism of 3-methylitaconate-delta-isomerase from *Eubacterium barkeri*. J Mol Biol. 2009; 391:609–20. https://doi.org/10.1016/j.jmb.2009.06.052 PMID: 19559030

46. Guzman LM, Belin D, Carson MJ, Beckwith J. Tight regulation, modulation, and high-level expression by vectors containing the arabinose PBAD promoter. J Bacteriol. 1995; 177(14):4121–30. PMID: 7608087